

Inter-planetary type-IV solar radio bursts: A comprehensive catalog and statistical results

ATUL MOHAN ^{1,2} NAT GOPALSWAMY ¹ ANSHU KUMARI ¹ SACHIKO AKIYAMA ^{1,2} AND SINDHUJA G ^{1,2,3}

¹NASA Goddard Space Flight Center, Greenbelt, MD 20771, USA

²The Catholic University of America, Washington, DC 20064, USA

³Bangalore University, Mysore Rd, Jnana Bharathi, Bengaluru, Karnataka, IN

(Received April 15, 2024; Revised May 20, 2024; Accepted May 31, 2024)

Submitted to ApJ

ABSTRACT

Decameter hectometric (DH; 1-14 MHz) type-IV radio bursts are produced by flare-accelerated electrons trapped in post-flare loops or the moving magnetic structures associated with the CMEs. From a space weather perspective, it is important to systematically compile these bursts, explore their spectro-temporal characteristics, and study the associated CMEs. We present a comprehensive catalog of DH type-IV bursts observed by the Radio and Plasma Wave Investigation (WAVES) instruments onboard Wind and STEREO spacecraft, covering the period of white-light CME observations by the Large Angle and Spectrometric Coronagraph (LASCO) onboard the SOHO mission between November 1996 and May 2023. The catalog has 139 bursts, of which 73% are associated with a fast ($> 900 \text{ km s}^{-1}$) and wide ($> 60^\circ$) CME, with a mean CME speed of 1301 km s^{-1} . All DH type-IV bursts are white-light CME-associated, with 78% of the events associated with halo CMEs. The CME source latitudes are within $\pm 45^\circ$. 77 events had multi-vantage point observations from different spacecraft, letting us explore the impact of line of sight on the dynamic spectra. For 48 of the 77 events, there was good data from at least two spacecraft. We find that, unless occulted by nearby plasma structures, a type-IV burst is best-viewed when observed within $\pm 60^\circ$ line of sight. Also, the bursts with a duration above 120 min, have source longitudes within $\pm 60^\circ$. Our inferences confirm the inherent directivity in the type-IV emission. Additionally, the catalog forms a sun-as-a-star DH type-IV burst database.

Keywords: Active sun(18) — Solar coronal mass ejections(310) — Stellar coronal mass ejections(1881)
— Solar radio flares(1342) — Space weather(2037) — Catalogs(205)

1. INTRODUCTION

Type-IV radio bursts were first classified in the meterwaveband by [Boischot \(1957\)](#). They appear as broadband continuum features in the dynamic spectrum and come in two flavours: stationary type-IV and moving type-IVs ([Takakura & Kai 1961](#); [Young et al. 1961](#); [Kundu & Spencer 1963](#)). A moving type-IV burst shows a clear drift in the dynamic spectrum while the stationary type-IV bursts do not. The sources of moving type-IV bursts were soon recognised to be moving away from the sun ([Weiss 1963](#); [Boischot & Clavelier 1968](#)). Using simultaneous white-light and radio (80 MHz) observations of the K-corona, [Hansen et al. \(1971\)](#) demonstrated that moving type-IV bursts are associated with bright coronal transients and derived a speed of 1300 km s^{-1} . Moving type-IV bursts were soon recognised as produced by flare accelerated electrons trapped in moving magnetised plasmoids associated with coronal mass ejections (e.g., [Takakura 1961](#); [Kundu & Spencer 1963](#); [Dulk & Altschuler 1971](#); [Smerd 1971](#); [Schmahl 1972](#)). [Robinson \(1978\)](#) performed a statistical analysis of 23 moving type-IV bursts observed by Culgoora radioheliograph and estimated the source speeds to lie within $200 - 1500 \text{ km s}^{-1}$. Meanwhile, the stationary type-IVs are produced by accelerated electrons trapped

in post-flare loops (see, Wild 1970; McLean & Labrum 1985, for an overview). The emission mechanism of the type-IV bursts are believed to be primarily via a plasma emission process based on observed polarisation and brightness temperature levels (e.g., Weiss 1963; Duncan 1981; Gopalswamy & Kundu 1989). Using 15 years of metric burst data from Culgoora radioheliograph, Cane & Reames (1988a) showed that $\sim 88\%$ of the 227 metric type-IV bursts, were associated with a type-II burst, which is produced by electrons accelerated by coronal mass ejection (CME) shocks (e.g. Smerd 1970; Wild 1970; Gopalswamy et al. 2005; Kumari et al. 2023). However, only around a third of the type-II bursts had a type-IV link. Type-IVs are closely connected to strong soft X-ray flares (on average with M class flares), especially ones which last for around an hour or longer, and fast CMEs (Cane & Reames 1988b). Similarly around 81% of the type-IVs in cycle 24 were found to be associated with white-light CMEs (Kumari et al. 2021). However, some of their cases of non-associations could be influenced by data gaps or stealth CMEs (e.g., Robbrecht et al. 2009; D’Huys et al. 2014; Morosan et al. 2021) which are known to have no white-light signatures. In such a case the percentage of association can increase.

Decameter-hectometric (DH) type-IV bursts are rare continuations of the metric type-IVs into the inter-planetary space, are almost always associated with fast ($>900 \text{ km s}^{-1}$) and wide ($>60^\circ$ angular extent) coronal mass ejections (CMEs) and there by to solar energetic particle events (SEPs) (Gopalswamy 2004, 2011; Hillaris et al. 2016). Unlike the metric type-IVs, DH type-IVs are always associated with CMEs that have a mean speed (V_{mean}) of $\sim 1500 \text{ km s}^{-1}$ and are $\sim 75\%$ of the time halo CMEs (Gopalswamy 2011). About 89% of these bursts are associated with GOES M- and X- class flares (Hillaris et al. 2016). Exploring the CMEs, between 1996 and 2006, that caused an SEP and a radio burst in the decimeter to kilometer (km) band, Miteva et al. (2017) showed that the median X-ray flare strength and CME speed are the highest for the events associated with DH - km type-IV bursts. DH type-IVs are observed below 14 MHz and occasionally extend down to 1 MHz with a mean extent down to $\sim 7 \text{ MHz}$ (Gopalswamy 2011). They last typically on average for an hour, occasionally extending over days (Hillaris et al. 2016). Since emission at frequencies below $\sim 10 \text{ MHz}$ cannot to be observed from ground due to ionospheric cut-off, these events can be detected only with space-based instruments (Gopalswamy 2011). The Radio and Plasma Wave Investigation (WAVES; Bougeret et al. 1995) instrument on-board Wind spacecraft and the SWAVES instrument on board Solar TERrestrial RELations Observatory (STEREO; Howard et al. 2008) spacecraft are the only window into this interplanetary radio emission. Despite the close association of DH type-IV bursts with SEPs, strong X-ray flares and fast and wide CMEs, there have been only a few studies of DH type-IV events compared to other type of solar radio bursts. This is primarily because these events are relatively rare (Hillaris et al. 2016), making it difficult to obtain a significant sample to explore their statistical behaviour in a robust manner. The results mentioned above on the DH type-IV bursts had only ~ 40 events mainly from just one solar cycle (C23) primarily from Wind spacecraft. Besides, Gopalswamy et al. (2016) had reported that the DH type-IV emission was directed within a cone angle of $\pm 60^\circ$ which is possibly associated with the line of sight occultation of the post flare loop by the solar disk. Using a few case studies with multi-vantage point data from Wind and STEREO missions Talebpour Sheshvan & Pohjolainen (2018) argued that the visibility of the the DH type-IV could be hampered by the presence of high density structures along the line of sight, which are formed by the interaction of the evolving CME with other pre-existing coronal magnetic field structures like streamers. These high density regions can attenuate the DH band radio emission from the post flare loop. However, to make robust conclusions on various characteristics of DH type-IVs and the properties of the CMEs/flares that correlate with the observed burst features, we need a statistically complete and significant sample.

In this work, we aim to put together a comprehensive sample of DH type-IV bursts detected by Wind and STEREO spacecraft, and catalog the properties of the associated CMEs. The catalog covers two full solar cycles (C23 and C24) and the start of the current cycle (C25), providing a statistically significant sample for exploration. The DH band spectro-temporal properties of these bursts will be explored alongside the properties of their associated CMEs. We will also address the issue of directivity in the events detected simultaneously by at least two widely-separated spacecraft. Recently, Patel et al. (2021) studied DH type-II radio bursts during the past two solar cycles. Since type-IV and type-IIs are generally considered as a radio diagnostic of strong CMEs this work will complement the aforementioned study forming a combined unique database to particle acceleration signatures of inter-planetary CMEs. Besides, type-IV radio bursts are the only solar-type bursts to be reported so far on other active stars (Zic et al. 2020; Mohan et al. 2024). Since our observations are full solar disk integrated emission, this database will form the first comprehensive sun-as-a-star catalog of interplanetary type-IV bursts.

Section 2 presents the sources of data while Sect. 3 describes the steps involved in identifying and compiling the DH type-IV events from the data sources. Section 4 presents the DH type-IV catalog and the statistical properties of these events. Section 5 analyse the results and discuss their implications. The conclusions are given in Sect. 6.

2. DATA

The data primarily comes from the compilation of the Coordinated Data Aanalysis Workshops (CDAW) Data Center¹. This work made use of the radio dynamic spectra from Wind, STEREO-A and STEREO-B spacecraft in the frequency range 0.02 - 14 MHz. The properties of the white-light CMEs observed by Large Angle and Spectrometric COronagraph (LASCO; Brueckner et al. 1995) onboard Solar and Heliospheric Observatory² (SOHO) are obtained from the LASCO CME catalog (Yashiro et al. 2004; Gopalswamy et al. 2009). We relied on the event reports from Space Weather Prediction Center³ (SWPC) to obtain the list of metric type-IV events since 1996. Besides, in some cases, we relied on various other public data sources to identify metric counterparts of DH type-IVs, namely eCallisto⁴, Radio Monitoring⁵ and Australian Space Weather Database⁶. The DH type-II catalog (Gopalswamy et al. 2019) compiled by CDAW Data Center is also used, since they are often associated with type-IVs and CMEs.

3. METHODOLOGY

We adopt a strategy of bias-free blind search for DH type-IV burst signatures. Since DH type-IV bursts are very closely associated with CMEs, the initial list of potential date-time periods to search for DH type-IV bursts was provided by the LASCO CME catalog. However, we may still miss some DH type-IV events due to potential data gaps in the LASCO data stream or due to events being not associated with white-light CMEs. To cover such periods and ensure sample completeness, we relied on two other catalogs of bursts potentially associated with DH type-IV bursts: metric type-IV event reports and the DH type-II catalog. Since DH type-IVs are continuations of metric type-IVs, the date-time periods from SWPC metric type-IV reports should provide a larger set of potential DH type-IV events. Nevertheless, the reason why we did not solely rely on the SWPC metric type-IV reports to search for DH type-IVs is that there have been cases where radio bursts go unreported in the SWPC event list. The DH type-II catalog, being an independent DH band catalog of CME associated radio bursts also provide additional date-time intervals helping us cover up for periods of LASCO data gap. The date-time interval we chose for the study extends from Nov, 1996 to May, 2023, which is when LASCO data started being available. This ensures that we have a well defined, systematically compiled catalog of CME characteristics covering multiple solar cycles (Yashiro et al. 2004; Gopalswamy et al. 2009). The final list of DH type-IVs search periods include date-times corresponding to 34083 LASCO CMEs, 939 metric type-IVs and 140 DH type-IIs.

A Python code was written to gather the dynamic spectra (DS) from Wind and STEREO for each date-time entry in the search list, by querying the respective databases^{7,8}. Whenever there is data from multiple missions, a combined DS is made. All the images were manually examined later to identify DH type-IV candidates. Figure 1 shows example DH dynamic spectra from periods with and without a type-IV event. After identifying the DH-type-IV candidates, the metric dynamic spectra were also accumulated for all events and ensured that there is a potential continuation of the DH type-IV into the metric band. We removed a couple of very long duration type-IV bursts extending over 10 h because of the difficulty in associating them with a particular CME event. These events can cause ambiguity in the scientific inferences derived on relationship between DH type-IV characteristics, particularly its duration and properties of associated CMEs. Thus we ended up with a preliminary sample of DH type-IV events, each of which is well associated with a CME. The preliminary DH type-IV sample was compared against existing event lists used by previous studies (Gopalswamy 2011; Gopalswamy et al. 2016; Hillaris et al. 2016) to ensure completeness across them. It was also ensured that the metric dynamic spectra, whenever available, from a ground based data repository had signatures of type-IV counterparts. Some spurious candidates with no clear metric counterparts were thus removed from the DH type-IV catalog.

4. RESULTS

¹ <https://cdaw.gsfc.nasa.gov/>

² <https://www.eoportal.org/satellite-missions/soho>

³ <https://www.swpc.noaa.gov/products/solar-and-geophysical-event-reports>

⁴ <https://www.e-callisto.org/links.html>

⁵ <https://secchirh.obsppm.fr/spip.php?rubrique8>

⁶ https://www.sws.bom.gov.au/World_Data_Centre/1/1

⁷ <https://cdaw.gsfc.nasa.gov/images/wind/>

⁸ <https://cdaw.gsfc.nasa.gov/images/stereo/>

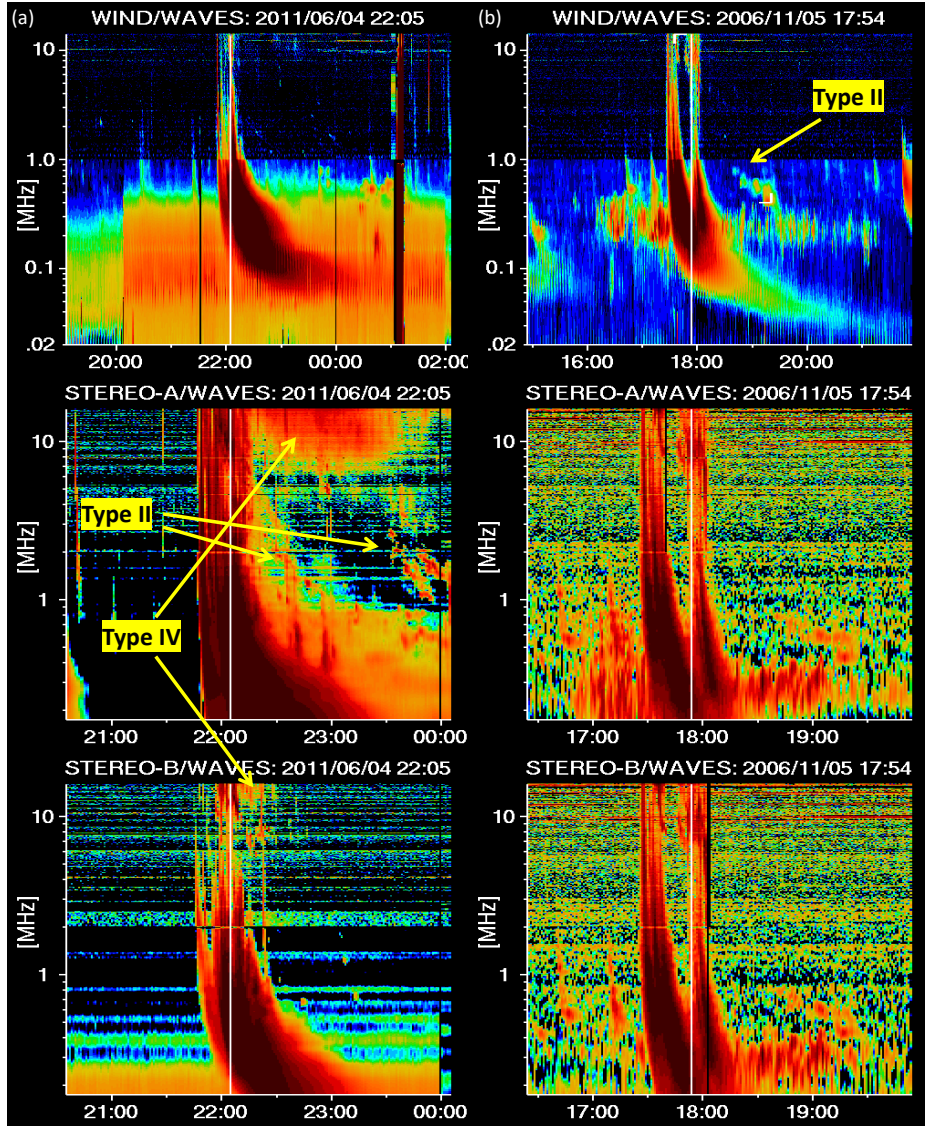


Figure 1. Example DH dynamic spectra. (a): A type-IV detection in STEREO-A and B. (b): No type-IV burst, but a type-II is detected by multiple spacecraft. The time periods of the associated LASCO CME events are marked by vertical white lines.

The final DH type-IV sample contains 139 events, each of which is well associated with a white-light CME. This is in contrast to the case of metric type-IV bursts which can occur without a white-light CME associated (Kumari et al. 2021). The sample has more events than previously reported for the specific periods covered by previous works. For instance, in 1998 - 2012 period we report 91 events as opposed to 48 reported by Hillaris et al. (2016). The rise in source count is partly because of the addition of data from STEREO spacecraft, unused in Hillaris et al. (2016). But, even if only the Wind/WAVES data within 1998 - 2012 are considered, our catalog has 71 events with a type-IV signature. Similarly, the current list has 65 Wind/WAVES events in cycle 23, compared to the 42 events reported by Gopalswamy (2011). This rise in the source count can be attributed to the blind search strategy employed by combining date-time periods across metric type-IV list, DH type-II catalog and the LASCO CME catalog. Also, the addition of STEREO data helped confirm some faint type-IVs in Wind/WAVES data which would have been omitted previously. Such faint events could then be confirmed based on the the detection of metric type-IV counterparts from ground based data.

Now that the authenticity of events in our sample and completeness across earlier catalogs are verified, we put together a catalog of the characteristics of these bursts in the radio DS, properties of the associated CMEs and the

flare location as recorded by multiple spacecraft. The latter gives a range of viewing angles for each event letting one explore the directivity of type-IV bursts. The following sub-section describes the contents of the catalog.

4.1. The DH type-IV catalog

(a) DH type-IV catalog

Type-IV properties										Type IV source view						Quality metrics		CME			Other info	
Date	Time	Dur (min)	End Freq (MHz)	M/S	Wind M/S	STA M/S	STB M/S	Best view spacecraft	Spacecraft	STB-Earth Angle (deg)	STA-Earth Angle (deg)	Src in Wind FoV (deg)	Src in STA FoV (deg)	Src in STB FoV (deg)	Event Quality	Data Quality	Date	Time	Flare loc	V_mean (km/s)	Solar Cycle	DH typell event
2023/04/21	18:24	36	9.7	S	S	S	NA	Wind	Wind;STA	5.9	-10.3	11	21.3	5.2	S2I2	W2A1B0	2023/04/21	18:12:06	S22W11	1284	25	Y
2023/03/06	11:04	59	12.6	S	S	NA	NA	Wind	Wind	7.6	-12.5	nan	nan	nan	S1I1	W2A2B0	2023/03/06	10:48:05	BL239	479	25	Y
2023/01/11	01:25	67	12.3	S	S	S	NA	Wind	Wind;STA	8.3	-13.6	-67	-53.4	-75.3	S2I1	W2A1B0	2023/01/11	01:25:53	N25E66	1083	25	N
2022/08/28	16:21	110	6.4	M	M	M	NA	Wind	Wind;STA	15.1	-20.1	85	105.1	69.9	S3I3	W2A2B0	2022/08/28	16:12:05	S30W85	1232	25	Y
2022/08/27	02:30	56	11	S	S	S	NA	STA	Wind;STA	15.3	-20.3	58	78.3	42.8	S2I3	W2A1B0	2022/08/27	02:24:06	S19W58	1284	25	Y
2022/08/18	11:15	28	11	M	M	M	NA	Wind	Wind;STA	16.2	-21.2	37	58.2	20.8	S1I2	W2A2B0	2022/08/18	11:00:05	S27W37	1327	25	Y
2022/07/08	21:25	62	9.2	S	S	NA	NA	Wind	Wind	20	-24.9	-40	-15.1	-60	S2I3	W2A1B0	2022/07/08	20:36:05	N20E40	1223	25	Y
2022/03/30	18:00	46	12.2	S	S	NA	NA	Wind	Wind	29.1	-32.9	31	63.9	1.9	S2I3	W2A1B0	2022/03/30	18:00:05	N13W31	641	25	N
2022/01/29	23:35	207	10	S	S	S	NA	STA	Wind;STA	31.9	-34.7	-6	28.7	-37.9	S2I3	W2A2B0	2022/01/29	23:36:06	N18E06	530	25	N
2017/09/17	12:05	55	7.9	M	NA	M	NA	STA	STA	128.6	-127.6	-170	-42.4	61.4	S3I3	W2A2B0	2017/09/17	12:00:06	S08E170	1385	24	Y
2017/09/16	11:55	256	3.4	S	NA	S	NA	STA	STA	128.6	-127.7	177	-55.3	48.4	S3I3	W2A0B0	2017/09/16	12:12:05	S04W177	325	24	N
2016/04/18	00:55	58	4.2	M	M	M	NA	STA	STA;Wind	152	-160.7	nan	nan	nan	S3I3	W2A2B0	2016/04/18	00:48:04	-----	1084	24	N
2016/02/21	12:00	100	9.9	S	NA	S	NA	STA	STA	159.2	-163.7	155	-41.3	-4.2	S3I1	W2A2B0	2016/02/21	12:00:04	N08W155	533	24	N
2015/11/04	14:14	27	5.9	M	M	NA	NA	Wind	Wind	174.4	-168.3	4	172.3	-170.4	S2I3	W2A0B0	2015/11/04	14:48:04	N09W04	578	24	Y

(b) Properties of CMEs associated with DH type-IV bursts

Date	DHtypeIV time	CME Time	Flare	PA (deg)	Width (deg)	V_mean (km/s)	V_fin (km/s)	V_20R (km/s)	accel (m/s ²)	M (g)	KE (erg)	MPA (deg)	Spacecraft	Remarks
2023/04/21	18:24	18:12:06	M1.7	Halo	360	1284	1100	1216	-28.1	nan	nan	180	Wind;STA	None
2023/03/06	11:04	10:48:05	---	233	45	479	554	576	7.2	nan	nan	229	Wind	None
2023/01/11	01:25	01:25:53	M2.4	67	89	1083	1033	1063	-6.7	nan	nan	72	Wind;STA	None
2022/08/28	16:21	16:12:05	M6.7	Halo	360	1232	1088	1168	-21.2	nan	nan	243	Wind;STA	None
2022/08/27	02:30	02:24:06	M4.8	Halo	360	1284	1198	1261	-12.1	nan	nan	225	Wind;STA	None
2022/08/18	11:15	11:00:05	M1.5	Halo	360	1327	1164	1216	-28.9	nan	nan	174	Wind;STA	None
2022/07/08	21:25	20:36:05	M2.5	Halo	360	1223	1051	1181	-23.3	nan	nan	77	Wind	None
2022/03/30	18:00	18:00:05	X1.3	Halo	360	641	573	531	-9.3	nan	nan	298	Wind	None; accel*1
2022/01/29	23:35	23:36:06	M1.1	Halo	360	530	434	379	-10.1	nan	nan	58	Wind;STA	None
2017/09/17	12:05	12:00:06	---	Halo	360	1385	1187	1308	-32.8	1.50E+16	1.50E+32	72	STA	None; M*2; KE*2
2017/09/16	11:55	12:12:05	---	112	8	325	272	51	-6.1	nan	nan	112	STA	Poor Event; accel*1
2016/04/18	00:55	00:48:04	---	275	162	1084	895	1041	-24.6	1.10E+16	6.30E+31	291	STA;Wind	Partial Halo; M*2; KE*2
2016/02/21	12:00	12:00:04	---	Halo	360	533	517	510	-1.7	3.60E+15	5.10E+30	298	STA	None; accel*1; M*2; KE*2
2015/11/04	14:14	14:48:04	M3.7	Halo	360	578	650	701	10.1	6.60E+15	1.10E+31	288	Wind	None; accel*1; M*2; KE*2

Figure 2. (a): A portion of the DH type-IV catalog. (b): The corresponding table of properties of the associated CMEs.

Figure 2a shows a portion of the DH type-IV catalog, the full version of which is published online⁹. Cross matching with the LASCO-CME catalog provided the properties of the associated CMEs (V_{mean} , acceleration, kinetic energy, mass and width), forming an additional table shown in Fig. 2b. A description of the catalog, the CME characteristics table and the dynamic spectra are published online¹⁰. The DH type-IV catalog is broadly divided into 5 sections, namely Type-IV properties, Type-IV source view, quality metrics, CME information and Other info. The first section provides the minimum frequency of emission and the time duration of emission at 14 MHz (referred to as duration hereafter). In cases where multiple spacecraft report on an event, the lowest observed minimum frequency and the longest observed duration are reported in the catalog. This procedure also helps us identify the spacecraft that recorded the ‘best view’ of the type-IV event. For instance, consider the event in Fig. 1a. The longest duration and the lowest minimum frequency is for the STEREO-A event which subsequently provided the best view of the burst compared to other spacecraft observations. The first section also classifies events into either moving (M) or stationary (S) type-IVs across spacecraft, while also mentioning the M or S classification in the best view spacecraft (in ‘M/S’ column). The second section in the table provides details of the multi-vantage point observations. The spacecraft that recorded the ‘best view’ is noted. Also, all the instruments that detected each event is reported in the ‘Spacecraft’ column. The relative positions of the spacecraft with respect to Earth is provided. Using the CME flare location obtained from LASCO CME catalog, the relative source locations in the visible solar disk of STEREO-A, STEREO-B and Wind spacecraft are estimated for each event. We use heliographic coordinates, so the source longitude ranges from -90° (east limb) to $+90^\circ$ (west limb) direction across the visible solar disk. Thus the relative location of type-IV bursts observed

⁹ https://cdaw.gsfc.nasa.gov/CME_list/radio/type4/DHtypeIV_catalog.html

¹⁰ https://cdaw.gsfc.nasa.gov/CME_list/radio/type4

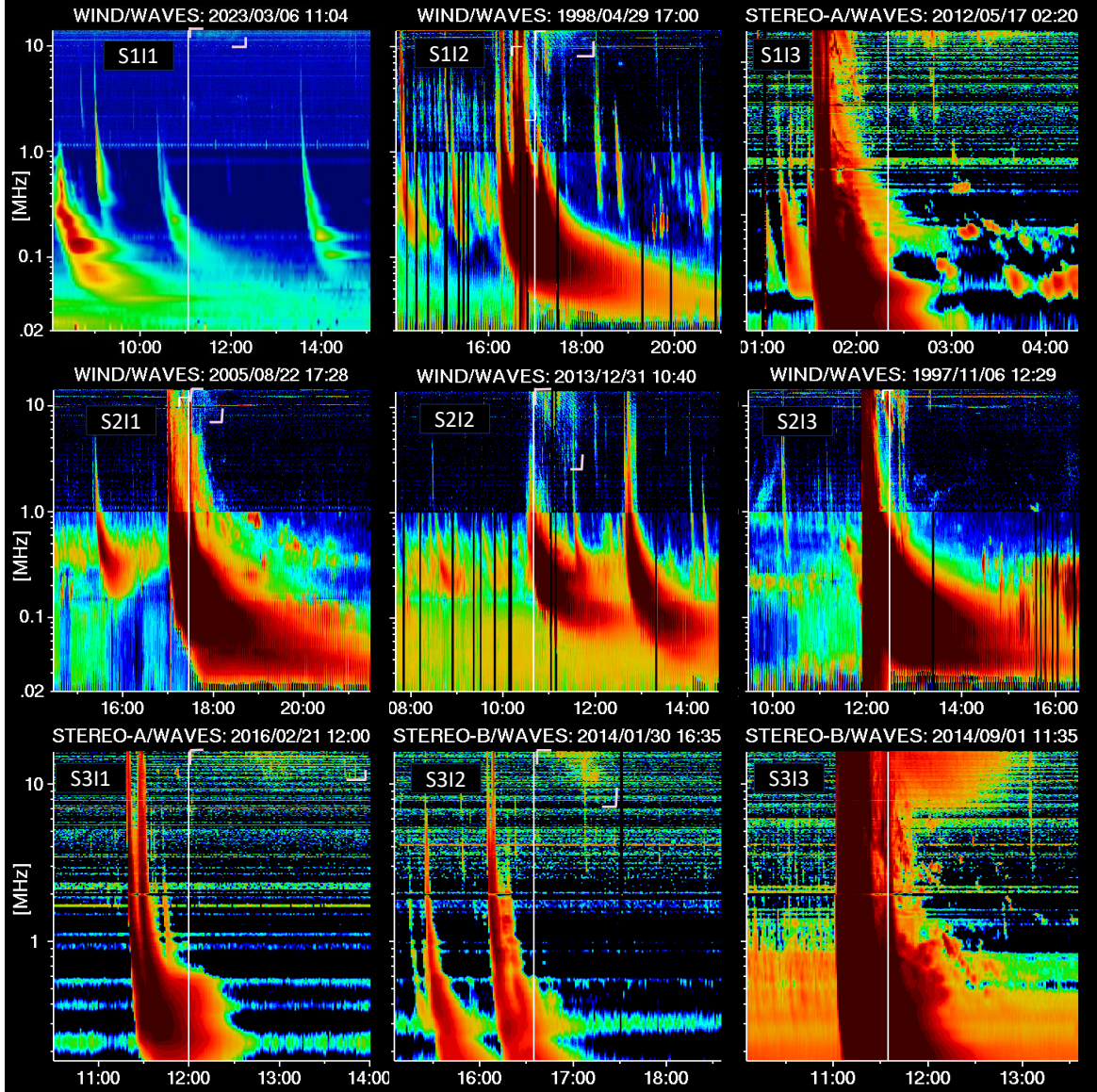


Figure 3. Collage of DH type-IV bursts varying in event quality, S_{ij} where $i,j \in \{1,2,3\}$ with 1 being worst and 3 being best. S refers to the morphology and I refers to the intensity of the events.

by multiple spacecraft provide a database to systematically explore emission directivity over our larger sample. The quality metrics will be introduced in detail in Sec. 4.1.1. In the CME section of the table, the date, time, flare location and the mean CME speed estimated are provided based on LASCO CME catalog. The ‘Other info’ section gives information on the solar cycle and on the association of DH type-II bursts. Combining all these information, we put together a comprehensive DH type-IV catalog for the period from 1996 to May, 2023, covering two full solar cycles and the rising phase of cycle 25.

4.1.1. Quality metrics

The DH type-IV catalog reports two quality metrics for each event, namely ‘event quality’ and ‘data quality’. ‘Event quality’ defines the quality of the detected type-IV event along two axes namely, shape (S) and intensity (I). The events reported by the best view instrument are ranked based on the dynamic spectral shape and intensity along an integer scale from 1 to 3. Note that 1 is the worst and 3 is the best. The ranking was done based on visual appearance. A type-IV burst is expected to appear as a broadband emission with a low-frequency cut-off. The cut-off can vary with time and the emission usually lasts for several minutes to hours. Based on how well the above features are traceable

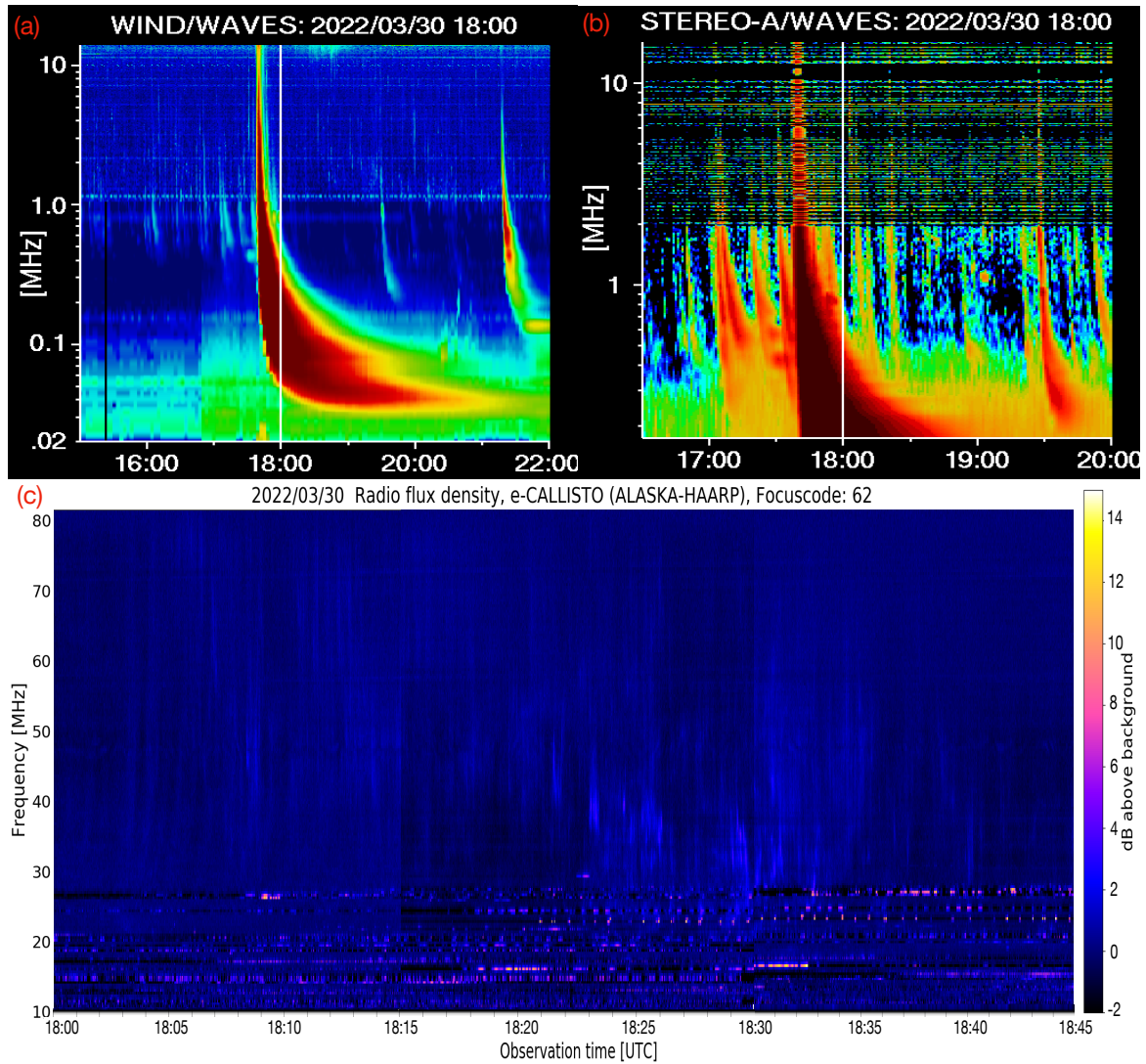


Figure 4. An example event with a data quality metric of W2A1B0. (a-b): DH type-IV is clearly detected by Wind/WAVES in >10 MHz between 18:00 - 19:00 UT on March 30, 2022 (W2); The quality of the STEREO-A data in 1 - 14 MHz is poor (A1), while STEREO-B was non functional during the period (B0). (c): A metric type-IV event recorded by e-CALLISTO station at Alaska. Data source: <http://soleil.i4ds.ch/solarradio/callistoQuicklooks/?date=20220330>

in the DS, the shape of the event is ranked. Since the burst morphology is often complicated in the frequency-time plane with multiple variability scales, defining a mathematical model is difficult. Also in many cases, the event is seen to be confined above 10 MHz making the shape identification and ranking hard. This is why a manual analysis mode was opted for. Now that we have a manually characterized set, this could be used for building AI/ML-based burst identification models in the DH band. Figure 3 shows a collage of selected spectra with varying event quality metrics. The square brackets mark the type-IV burst emission. Consider the top row in the figure. Moving from I1 to I3 the intensity of the type-IV emission can be found to increase with respect to the background making it easily discernible. However, note that the morphology of the emission is not well defined and these events are hence identified based on co-observations from other spacecraft and metric band DS from ground-based telescopes. Direct observation of a post-flare loop that brightens up in co-temporal X-ray images was used as supporting evidence, increasing the likelihood of the emission being a type-IV, in cases of weak events. Now, consider the rightmost column in the collage. The relative intensity of the emission is very high (I3). As we move from top to bottom, the type-IV emission structure can be found to become clearer as the minimum frequency of the emission extends to lower frequencies in the observing window. This effect can be seen moving down the other two columns as well. Note that the middle column shows

	Property	All events		Non -halo CMEs	
		Mean	Median	Mean	Median
DH type-IV	Duration (min)	83.8	62	93.1	59
	Min. frequency (MHz)	7.8	7.5	7.4	7.2
CME	Vmean (km s^{-1})	1301	1223	932	874
	Width (deg)	310	360	135	120

Table 1. Statistics of the various properties of DH type-IVs and associated CMEs. Characteristics of events associated with non-halo CMEs (width $<300^\circ$) are separately provided. 102 out of 139 events were non-halo CMEs.

different moving type-IV events. In this scale, the event in Fig. 1a middle panel would be ranked S3I3 due to the distinctive type-IV shape and intensity contrast, while the STEREO-B event would be S3I1. However, the catalog would report event quality as S3I3 corresponding to the best detection. The spacecraft with the best quality detection is reported as the ‘Best view spacecraft’ (see, Fig. 2(a)). We note that events with good ‘S’ metric are usually the ones that extend below 10 MHz in the dynamic spectrum and appear relatively isolated in the dynamic spectrum from other bursts, both aiding in detecting and characterizing them better. Often when a type-IV burst is not well isolated in the DS, despite its frequency extent or duration, it could get a ‘shape’ metric of 2 rather than 3. A shape metric of 1 could suggest that the event was either in a very crowded part of the DS interlaced with several other bursts, or the event did not extend much in the frequency and time axes to discern the shape well.

The ‘data quality’ metric rates the quality of the DS data recorded by all spacecraft, during a burst event. The spacecraft are tagged by letters W, A and B for Wind, STEREO-A and STEREO-B, respectively. The metric is formed by combining the letter tag with an integer quality metric. The integer metric is either 0, 1 or 2 denoting the absence of spacecraft data, the existence poor quality data or the availability of good quality data. Fig. 4a-b shows an event where a DH type-IV is detected by Wind in the high frequency channels. Meanwhile, the $\sim 2 - 14$ MHz data recorded by STEREO-A is of poor quality to make a robust conclusion. The source was at 63.9°W in the STEREO-A field of view. STEREO-B was non-functional during the period. Fig. 4c shows a simultaneous metric dynamic spectrum showing the event during the same period, from an e-CALLISTO station at ALASKA. Meanwhile, the two events shown in Fig. 1 are ranked W2A2B2 since the data quality is good in all spacecraft irrespective of the detection of type-IVs. The two metrics are crucial for identifying reliable, good quality observations by multiple spacecraft, for a statistical study of the effect of line of sight in the observed radio burst characteristics. However, to explore the mean statistical properties of DH type-IV bursts one can use the values in the Type-IV properties section which is by definition is based on the ‘best view’ instrument data.

4.2. Characteristics of DH type-IV bursts and associated CMEs

Figure 5a shows the histograms of minimum frequency and duration at 14 MHz for all 139 events, while the bottom panel of the figure shows the mean velocity and angular width of the associated CMEs. Note that 8 events did not have good LASCO data, either due to data gap or saturation effects from the bright event, which reduced the number of events to 131 in our CME statistics. However, a CME is detected in all of these 8 events in the extreme Ultraviolet and X-ray images.

Table 1 shows the statistics derived from the property distributions in Fig. 5. The median values of duration and minimum frequency are 62 min and 7.5 MHz respectively, while the associated CMEs showed a median V_{mean} of 1223 km s^{-1} with $\sim 78\%$ [102 out of 131] of them being halo CMEs (e.g., Howard et al. 1982; Zhou et al. 2003; Gopalswamy et al. 2007). Halo CMEs are wide events seen extending around the entire occulting disk of the coronagraph. There is no significant difference in the mean properties of the DH type-IV bursts associated with non-halo CMEs and the larger sample. However, the mean CME speed of non-halo CMEs causing the DH type-IV bursts is around 932 km s^{-1} compared to the full sample mean of 1301 km s^{-1} . Meanwhile, halo CMEs can be a disk centre event, a limb event or a backside event (Gopalswamy 2004). However, since the post-flare loops and moving plasmoids in backside events will be mostly occulted by the disk, only the DH type-IV bursts associated with front-side or limb events are observable. Figure 6(a) shows the distribution of DH type-IV sources on the solar disk as seen by multiple instruments. The dashed bold longitudes mark the $\pm 60^\circ$ region. About 82% of the sources are concentrated within this region, demonstrating a strong directivity in the longitude distribution of these events. The source latitudes are clearly within $\pm 30^\circ$, indicating that the underlying CMEs originate from the active region belt. Only active regions

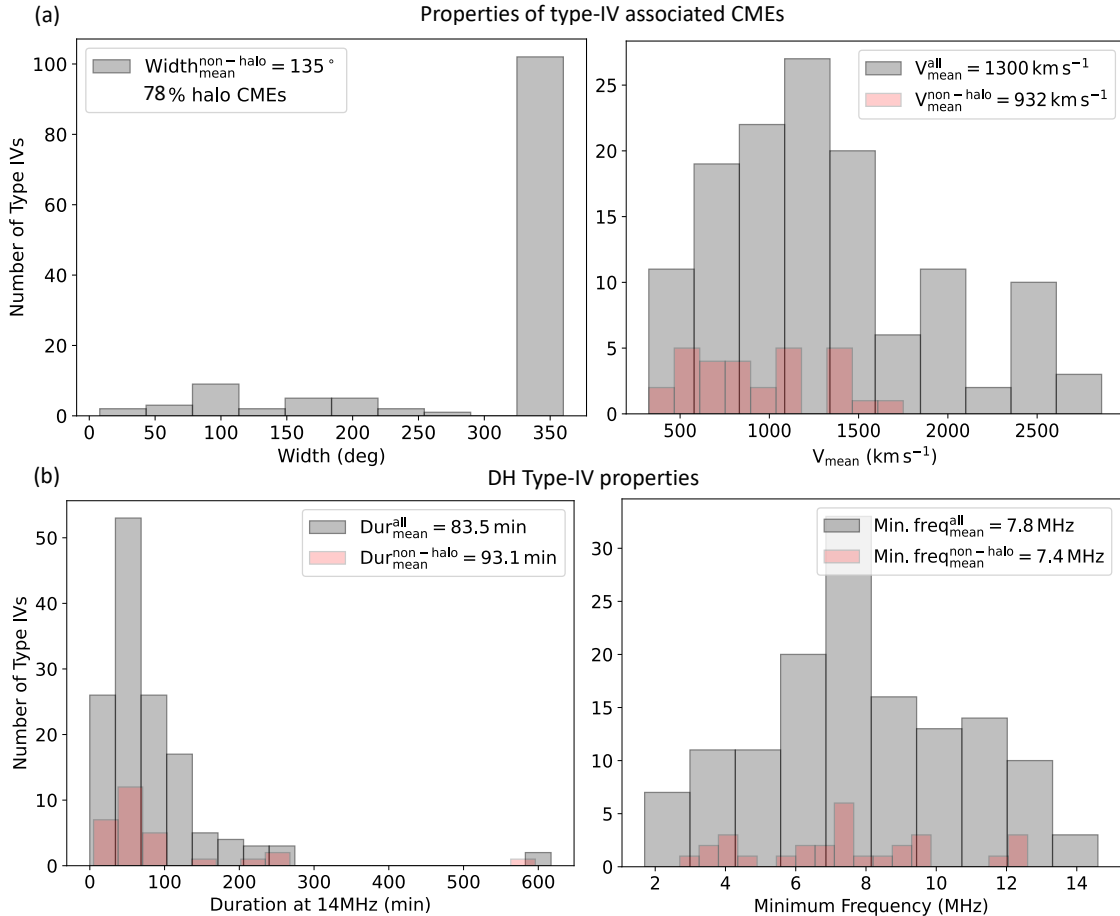


Figure 5. (a): Properties of the CMEs associated with the DH type-IV bursts. 78% of the events are halo-CME associated. (b): Properties of the DH type-IV bursts. Legends show the mean values of each property for all bursts and for those associated with non-halo CMEs. The mean properties of DH type-IV bursts caused by non-halo CMEs are similar to the full sample. But, the V_{mean} is slightly lower for the non-halo events.

have the ability to produce powerful CMEs that produce DH type-IV bursts. The other panels in Fig. 6 show the same information on the source distribution as, but the marker sizes represent minimum frequency (b) and the duration of the burst. The sizes are denoted on a scale relative to their respective maximum property value. The size distribution has no clear dependency on the latitude or longitude of the burst sources.

5. DISCUSSION

The mean CME and radio burst properties listed in Table. 1 agrees with the previous results by other authors within a few % (Gopalswamy 2011; Hillaris et al. 2016), except for V_{mean} . Gopalswamy (2011) reported a mean V_{mean} of 1526 km s^{-1} , compared to our value of 1301 km s^{-1} . Also, we find a 32% association of DH type-IVs with CMEs having $V_{\text{mean}} < 1000 \text{ km s}^{-1}$, as opposed to 20% (Gopalswamy 2011) and 26% (Hillaris et al. 2016) association reported earlier. It is possible that our blind search criteria combining multi-spacecraft data helped nearly triple the number DH type-IV bursts, with more events associated with weaker CMEs providing a more statistically complete dataset. However, we broadly agree with the inferences of the earlier publications that DH type-IV bursts typically last for over an hour, extending on average to frequencies $\approx 7.5 \text{ MHz}$ and are commonly associated with fast ($> 900 \text{ km s}^{-1}$) and wide ($> 60^\circ$) CMEs. 96 out of 131 bursts (73%) with a well identified source location, have a fast and wide CME association. Also, 78% (102 out of 131) of the bursts are associated with a halo CME. We explored the non-halo CMEs associated with DH type-IV bursts separately. The mean speed and the width of these CMEs also fall well within the definition of a fast and wide CME. Figure 7 shows the solar cycle variation in the DH type-IV detection count from the vantage point of the Earth, as seen by Wind/WAVES. The number of type-IVs clearly follow the variation in

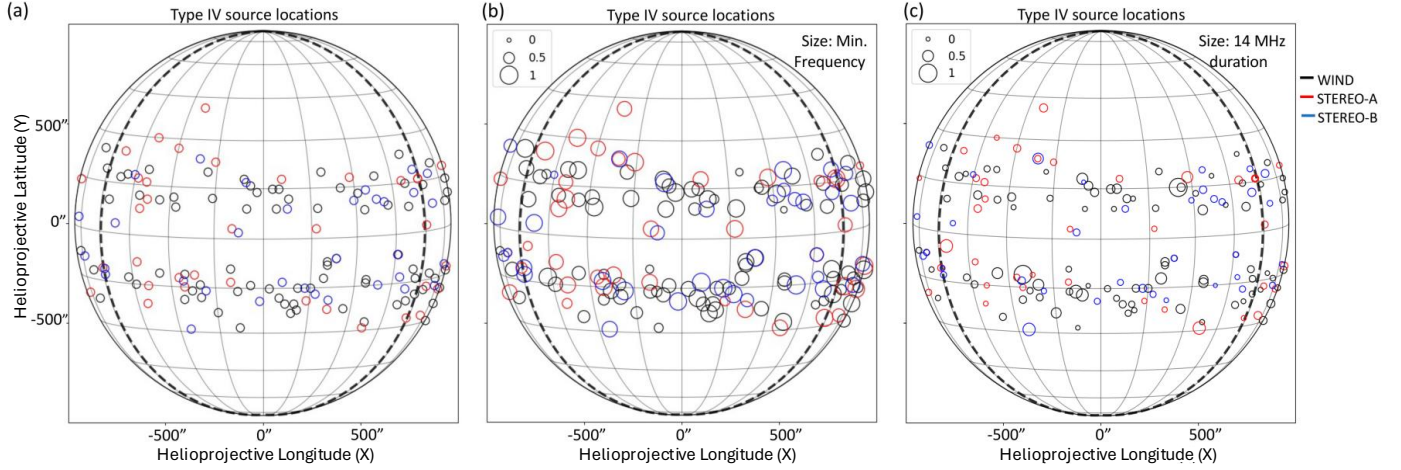


Figure 6. Stonyhurst maps showing the location of the active regions associated with DH type-IV bursts, in the field of view of each spacecraft. (a): Colors denote different spacecraft. 82% of the type-IV sources lie within $\pm 60^\circ$ longitude, demarcated by the thick dotted great circles. The source latitudes, except in one case, are confined within $\pm 30^\circ$. (b-c): Same information as (a) with the marker size denoting the minimum frequency and the duration of the burst on a scale relative to the respective maximum value. Neither minimum frequency nor duration show a clear preference to source location.

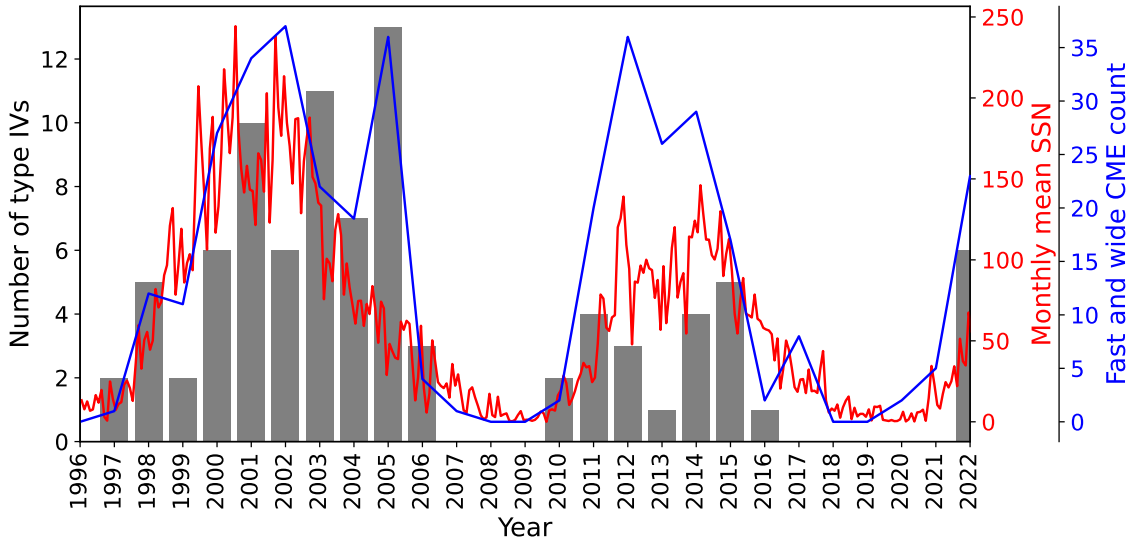


Figure 7. Solar cycle variation in the number of DH type-IV bursts observed by Wind/WAVES. Monthly mean sunspot number (red) and the number of fast and wide CMEs (blue) are shown. 73% of the DH type-IV bursts in the catalog are associated with a fast and wide CME.

the number of fast and wide CMEs. Though it follows the monthly mean sunspot number, the correlation is stronger with the number of fast and wide CMEs. This is evident from the fact that the type-IV counts even follow the bump around 2005 - 2006 period and the dip around 2013 seen in the fast wide CME counts. However, despite this strong generic association between two, the number of fast and wide CMEs is much higher than that of the DH type-IV bursts. In fact, within Nov 1996 to May 2023, only 18% of the fast halo CMEs produced a DH type-IV burst. This means that even if a CME with the most favourable physical attributes occur in terms of speed and angular extent, the odds for an associated DH type-IV burst is fairly low. Besides, DH type-IV bursts show a 67% (93 out of 139 events) association with DH type-IIIs.

5.1. Longitude of type-IV burst sources - emission directivity

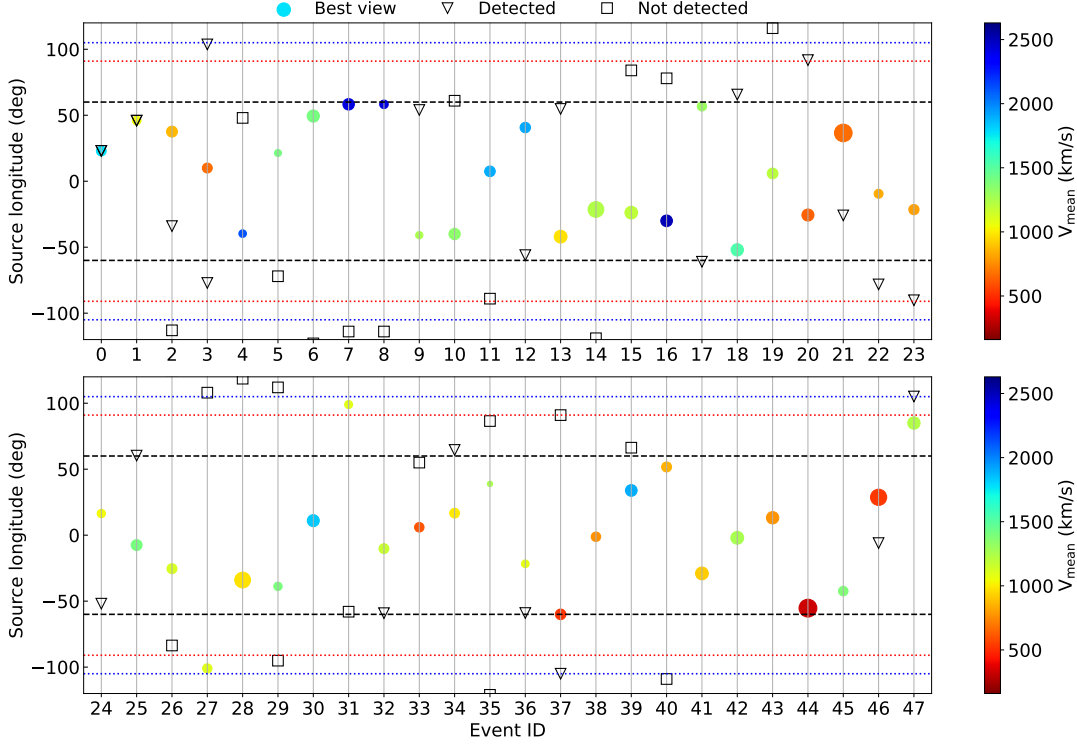


Figure 8. All 48 events that had good observations from at least 2 spacecraft. X-axis shows a representative event ID for each event. Y-axis shows the burst source longitude relative to the spacecraft vantage point. The relative source longitudes that gave a detection are marked by triangles and circles, with circles marking the best detection. The size of the circle represent the burst duration while the color denote V_{mean} . Dashed horizontal lines mark $\pm 60^\circ$, $\pm 90^\circ$ and $\pm 105^\circ$ longitudes. Longitude $> |90|$ represent flare sources behind the limb. In some cases where the post-flare loop rose much higher, a type-IV emission could be detected from flare sources slightly behind the limb.

As mentioned earlier, [Gopalswamy et al. \(2016\)](#) showed that the type-IV burst sources appear to be concentrated within $\pm 60^\circ$ longitude. However, this was based on type-IV burst location distribution derived from cycle 23, a period before the STEREO era. So also they did not have a sample of multi-vantage point observations of type-IV bursts to verify the directivity in a systematic manner. However, the authors presented a single case study of an event from 2013 Nov 7 that was observed with the Wind and STEREO spacecraft. The DH type-IV event was found to be best observed by the spacecraft which was viewing the event within $\pm 60^\circ$. Based on this the authors argued that there could be a directivity in the inherent emissivity, besides any effect due to background plasma opacity. A few case studies that followed this paper, argued that occultation by dense overlying material, often a CME-streamer shock formed towards the CME flank region, could be prime reason for the blocking the emission along certain viewing angles and not necessarily inherent emissivity ([Melnik et al. 2018](#); [Talebpour Sheshvan & Pohjolainen 2018](#); [Pohjolainen & Talebpour Sheshvan 2020](#)). Thus the earlier studies that explored directivity in the emission have either been on specific cases or on the distribution of observed source locations from one spacecraft without factoring in the variation in the dynamic spectral morphology detected from multiple vantage points. The DH type-IV catalog presented here, has event and data quality metrics which grades the characteristic detail in the observed DS of each DH type-IV event for each spacecraft located at different vantage points. Based on these metrics, the catalog also mentions the best-view spacecraft which detected the type-IV burst with the best extent in frequency and time of all recorded data from multiple view points. This let us study the direction dependency in not only the detection of the DH type-IV burst, but also its morphological details in the DS.

To systematically explore the effects of viewing angle, the bursts detected with a good event quality of $\text{SI}ij$, where $i, j \in \{2, 3\}$ were first chosen. From these events, only those that occurred when at least two spacecraft were producing good dynamic spectra with data quality of 2 were chosen. This produced a subset of 48 events with good multi-vantage point observations of the Sun from at least two viewpoints. The list of events with burst and CME characteristics

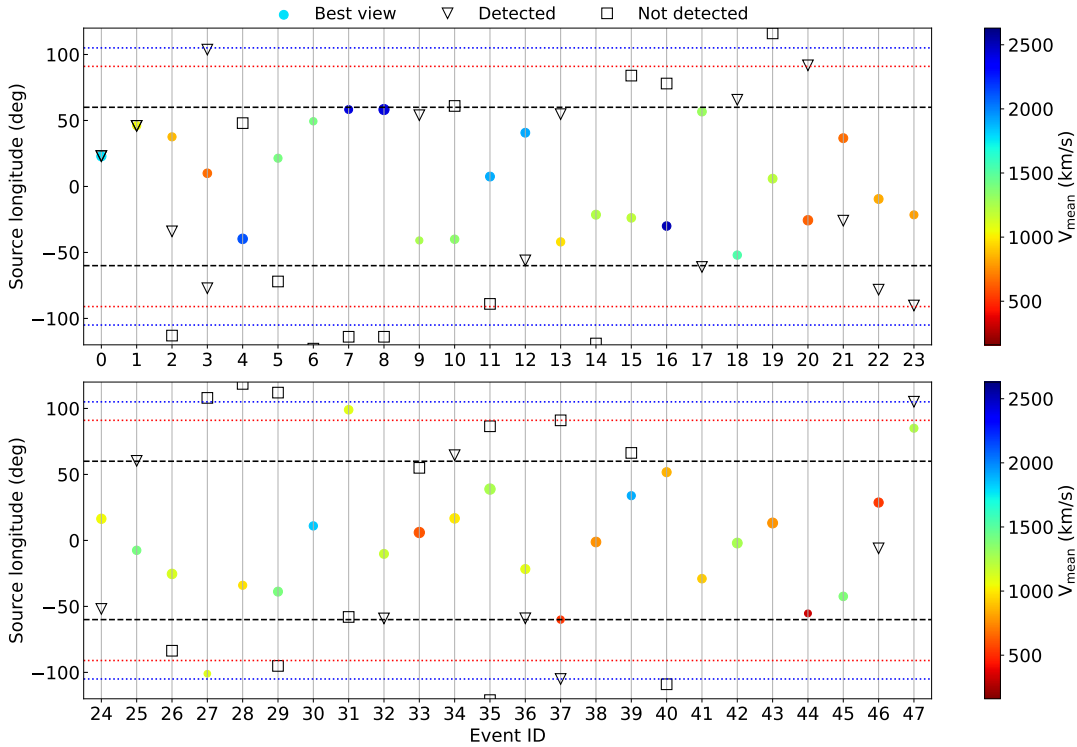


Figure 9. Same as Fig. 8. Sizes of the circles represent minimum frequency.

and assigned event IDs are provided online¹¹. The event ID simply tags each event. Figure 8 shows the expected source longitudes of the selected DH type-IV burst sources (i.e. flare loops) in the frame of each spacecraft. Locations of the best-observed burst events are marked by colored circles, other detected source longitudes by triangles, and non-detections by squares. The non-detection longitudes provide the source location of the associated flare in the reference frame of the spacecraft which failed to detect it. Marker colors of the best-viewed detections denote V_{mean} and sizes denote the type-IV duration. Figure 9 is similar to Fig. 8 with the exception that the sizes denote minimum frequency. First, the role of viewing angle (or apparent source longitudes) in the detection of DH type-IV bursts is explored. We find that 58 out of 62 observations (94%) made within $\pm 60^\circ$ source longitude by various spacecraft detected a burst (see, circles and triangles). Meanwhile, only 9 out of 20 observations (45%) made between $\pm 60^\circ$ and $\pm 105^\circ$ were detections. Of the total type-IV detections reported when the spacecraft are viewing the source at an angle within $\pm 105^\circ$, only 13% (9 out of 67) is contributed by spacecraft view points $> |60^\circ|$. An upper limit of 105° is set on the source longitude because of a few type-IV detections associated with flares that occurred slightly behind the limb. The post-flare loops or plasmoids that caused the radio burst in these events extended sufficiently beyond the limb making them visible, as evidenced by the associated extreme Ultraviolet (EUV) movies. For instance, Event 47 was detected by two spacecraft, both viewing it close to the limb with flare source longitudes of 85° and 105° . Figure 10 shows the DS for the event along with EUV and white-light coronagraph images from the two spacecraft that detected it. The EUV and coronagraph images correspond to the time instants marked by the lines in the DS. A post-flare loop can be found rising beyond the limb in the EUV images. This implies that the DH type-IV bursts are detectable even beyond the the limb ($> 90^\circ$ source longitude), provided the post-flare loop is visible over the limb and there are no dense occulting structures along the line of sight. From Fig. 8, only 3 detections are reported out of the 14 such observations from $\gtrsim 90^\circ$ source line of sight.

Now we explore the effect of viewing angle in the observed morphology in the radio DS. From Fig. 8, it can be seen that for every event the spacecraft which recorded the best view (marked by circle) was always within $\pm 60^\circ$ longitude, provided there was a spacecraft observing the source within that range. The only exception for this rule is Event 31, which was hence studied in detail. Figure 11 shows the observations of the event in radio, EUV and white-light

¹¹ https://cdaw.gsfc.nasa.gov/CME_list/radio/type4/All_good_multiview_events.html

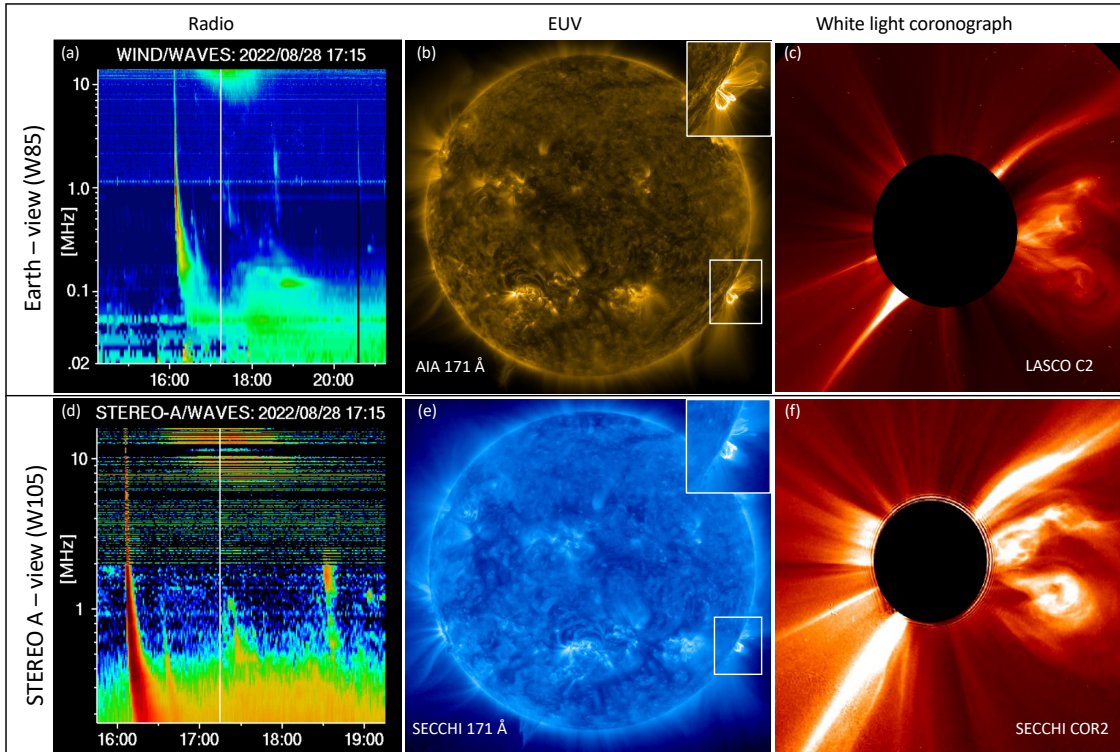


Figure 10. Case of a type-IV from a flare source behind the limb (Event 47): Radio, EUV and white-light coronagraph observations of a limb CME event from the view points of the Earth (top row) and STEREO-A (bottom row). Source locations are specified in the left of each row (Wind: 85°W ; STEREO-A: 105°W). STEREO-A was at 20°E with respect to the Earth. DH type-IV burst was observed by both spacecraft. Associated post-flare loop is visible over the limb in the EUV maps from both vantage points. The insets in the middle panel zooms in to the loop region. The rightmost panels show the CME in the coronagraphs from the Earth and STEREO-A vantage points.

coronagraph as seen from the viewpoints of the Earth (Top row) and STEREO-B (Bottom row). A DH type-IV burst was detected by STEREO-B but not by Wind, despite the latter viewing the source at $\sim 60^\circ$. Meanwhile, for STEREO-B this was a limb event. The post flare loop is clearly visible at the limb from the STEREO-B viewpoint as seen in the 171\AA image from SECCHI instrument on board STEREO-B. The inset of Fig. 11(e) shows a zoomed in image of the region. However, the 171\AA image of the flaring region as seen from Earth, taken by AIA onboard SDO, reveal a complex active region configuration (Fig. 11(b)). The insets in the panel zooms into the flaring active region in 171\AA (top right) and HMI continuum (bottom right) maps. The HMI map reveals a complex $\beta\gamma$ sunspot group near the flare site. Also, another active region can be spotted (marked by arrow) within 10° separation of the one in question. Hence, given the complex magnetic field configuration in the neighborhood of the flare site, the radio bursts are likely occulted by the dense plasma in the complex post eruption field structures. The effect of source occultation on type-IV burst detection has been discussed in earlier works (e.g. Talebpour Sheshvan & Pohjolainen 2018; Pohjolainen & Talebpour Sheshvan 2020). This occultation effect could also be the cause of the disruption of the type-I noise storm in the Wind DS after $\approx 16:20$ UT, when the CME associated type-III burst occurred. Meanwhile, the type-IV burst recorded by STEREO-B is a moving type-IV and starting around 16:50 UT when the plasmoid structure marked by white arrow in Fig. 11(f) first appears in the SECCHI COR2 field of view.

The inferences from the overall statistics and the special case of Event 31 suggest that in the absence of dense structures along the line of sight that can occult the view, a DH type-IV burst is best viewed when the spacecraft is within $\pm 60^\circ$ LOS. However, DH type-IV bursts can be detected even from limb sources when there is no significant

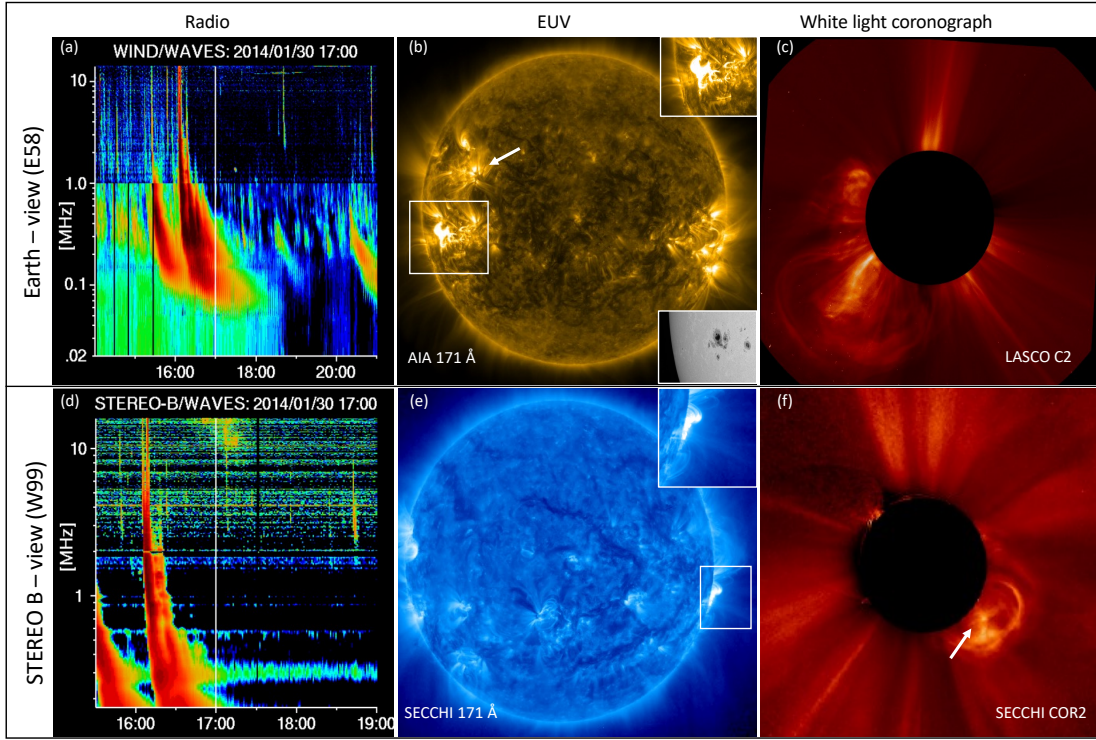


Figure 11. Case of Event 31: Radio, EUV and white-light coronagraph observations of the CME from the view points of the Earth (top row; source longitude: 58°E) and STEREO-B (bottom row; source longitude: 99°W). STEREO-A was at 150°W with respect to the CME source. DH type-IV burst is detected by STEREO-B but not Wind. Insets in the top right region of the middle panels (b and e) zooms in to the white boxes that mark the flaring region. In panel b, a HMI image of the flaring region is provided in bottom right inset. The arrow in panel b marks the nearby active region while in panel f, the arrow points at the CME plasmoid temporally correlated with the observed DH type-IV. The active region marked in panel b is the likely source of the noise storm in Wind/WAVES in the pre-flare period (before $\sim 16:00$ UT). STEREO-B does not detect this emission possibly because of the directivity weakening the flux density of the noise storm source which is only partly visible at the limb in STEREO-B field of view.

LOS occultation (e.g., Event 47), though this need not be the line of sight that provide the best view of the event. This is as expected from the hypothesis of (Gopalswamy et al. 2016) that the type-IV emission could have inherent directivity in the emission making it best viewed within $\pm 60^\circ$ line of sight out of all possible detections in different lines of sight.

5.2. Relations between DH type-IV properties, associated CME and viewing angle

Since the viewing angle or equivalently the observed source longitude is a crucial factor in obtaining the best view of the burst, it is possible that the properties of the radio burst in the DS might depend on source longitude. But, the colors and sizes of the circles in Fig. 8 and Fig. 9 do not show any particular pattern in their distribution across the longitude axis. Since the colors denote V_{mean} , this means that the CME speed is not a crucial determinant in deciding the detectability of a type-IV burst even close to the limb. Similarly, the duration (in Fig. 8) and minimum frequency (in Fig. 8) of the radio burst denoted by the sizes, also do not show any definitive trend across longitude axis. This means that the emission directivity may not have a major impact on the observed DS characteristics. We further explored the patterns and inter-relations, if any, in the multi-parameter space of the properties of the observed type-IV burst, associated CME and viewing angle. Only events with event quality, SiIj such that $i, j \in 2, 3$ were chosen for this study. Figure 12 shows the variation in V_{mean} , type-IV duration, minimum frequency and best-view source longitude for all selected events. We use the absolute value of the source longitudes since the effect of viewing angle

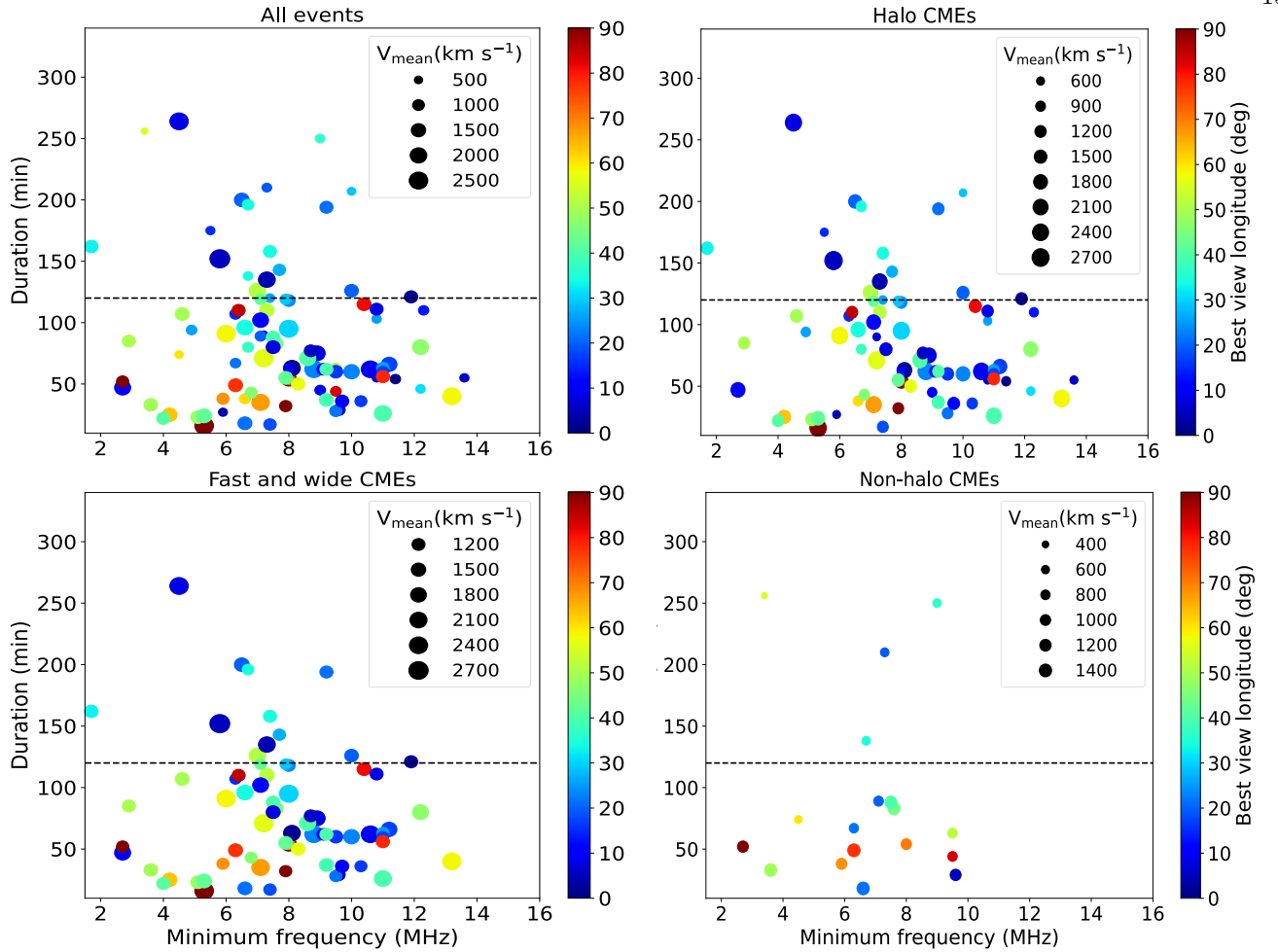


Figure 12. Properties of DH type-IV events with quality of at least SiIj, where $i,j \in 2,3$. Modulus of source longitude is shown in color scale, while sizes denote V_{mean} . Horizontal line marks 120 min.

should be symmetric about the central meridian. Different panels explore the event characteristics for halo, non-halo and fast-wide CME associated events. Halo and non-halo CMEs were separately studied because the CME width histogram in Fig. 5(b) shows a bimodal distribution. Also, the fast-wide CMEs were explored separately since their occurrence rates are seen to correlated well with that of DH type-IV counts (see, Fig. 7). The detection of DH type-IV bursts with duration longer than 120 min (horizontal black line) seems to prefer a source longitude within $\pm 60^\circ$. A more detailed clustering analysis is currently underway by expanding the CME property table (Fig. 2(b)) with more physical characteristics of the CME and associated flare. This is beyond the scope of this paper which is aimed at presenting the catalog, statistics, type-IV directivity and preliminary inferences on clustering of various properties of these events.

6. CONCLUSION

We present a comprehensive catalog of Decametric Hectometric (DH) type-IV bursts during the period between Nov, 1996 and May, 2023, covering two complete solar cycles (23 and 24) and the rising phase of the current cycle. The catalog is complete to the entire LASCO CME event list and also covers the period of reported metric type-IV and DH type-II bursts. All DH type-IV bursts are associated with white-light CMEs, in contrast to the case of metric type-IV bursts. Also, we include radio data gathered by three spacecraft namely Wind, STEREO-A and STEREO-B. This not only help increase the source count, but also provides multi-vantage point observations for several DH type-IV bursts letting us explore the intriguing aspect of emission directivity. The final catalog has 139 DH type-IV bursts, along with the properties of the associated CMEs. Since DH band dynamic spectrum is a disk integrated observable,

the presented catalog form a sun-as-a-star database to explore the CME-related type-IV bursts, which are one of the much sought after radio signatures of stellar-CMEs.

DH type-IV bursts are mostly associated with halo CMEs (78%; 102 out of 131 events) with a mean speed of 1301 km s^{-1} . 93 out of 139 events had a DH type-II association. The solar source longitudes of the detected events lie within $\pm 60^\circ$ for 58 out of 62 cases where multiple spacecraft observed the same source from different vantage points. The source latitudes of all except one type-IV source is found to be within $\pm 30^\circ$ latitude pointing at the association of strong CME causing active regions with DH type-IV bursts. The sole outlier is however within $\pm 45^\circ$. Our statistical results over a sample thrice larger than previous studies confirm the earlier results by different authors (e.g. Gopalswamy 2011; Gopalswamy et al. 2016) in a statistically robust manner. We find a strong correlation between the occurrence of these bursts with that of the fast and wide CMEs during the catalog period. However only 18% of the fast halo CMEs that occurred during the catalog period produced a DH type-IV burst. So a DH type-IV detection indicates a high likelihood for the occurrence of a fast halo CME, but the converse is not true.

Using the multi-vantage point observation data from Wind and STEREO spacecraft, the effect of directivity on the detection of these bursts and on their observed morphology in dynamic spectrum (DS) were explored. When 94% of cases where the spacecraft was observing a flare source within $\pm 60^\circ$ line of sight, ended up in a detection, only 45% of the observations made outside this field of view reported a burst. In cases where multiple spacecraft observed an event, it is found that the spacecraft which observed the burst source within $\pm 60^\circ$ longitude recorded the burst with the longest duration and extending down to the lowest frequency in the DS whereby providing the best or most detailed view of the event. This rule had only one exception in the entire catalog, in which case we find evidence for significant occultation of radio emission by surrounding magnetic field structures. However, in the absence of significant line of sight occultation, type-IV bursts from even limb events can be detected, though these detections may not provide the best possible view of the event. Additionally, the detection of a burst with duration > 120 min strongly prefer a viewing angle within $\pm 60^\circ$. Based on these results we infer that, though detecting a DH type-IV is possible at source longitudes extending up to the limb, a comparison of the dynamic spectra for the same burst as seen by multi-vantage point missions do suggest an inherent directivity in the radio emission that prefer $\pm 60^\circ$ viewing cone as hypothesised by Gopalswamy et al. (2016).

We thank the CDAW team for maintaining an up to date catalog of LASCO/CME events and processed dynamic spectra from Wind and STEREO spacecraft. We also thank SWPC, Radio Monitoring, Australian Space Weather Data Center and eCallisto network for the open access database they maintain for various solar events. AM acknowledges the discussions with Sunpy team via Elements¹² platform. AK's research was supported by an appointment to the NASA Postdoctoral Program at the the NASA Goddard Space Flight Center (GSFC). AM and NG are supported in part by NASA's STEREO project and LWS program. SA was partially supported by NSF grant, AGS-2043131. SG's research was supported by NSF grant, AGS-22289. AM acknowledges the developers of the various Python modules namely Numpy (Harris et al. 2020), Astropy (Astropy Collaboration et al. 2013), Matplotlib (Hunter 2007) and multiprocessing. AM also thanks the developers of CASA (McMullin et al. 2007). AM acknowledges the help from Seiji Yashiro in posting the catalog online and for maintaining the various CDAW data resources. AM acknowledges Pertti Mäkelä for useful discussions and sharing of data.

Facilities: Wind (WAVES), STEREO (SWAVES), SOHO (LASCO), SDO (AIA)

Software: Numpy (Harris et al. 2020), Astropy (Astropy Collaboration et al. 2013), Matplotlib (Hunter 2007), Multiprocessing (McKerns et al. 2012), Pandas (pandas development team 2020), Urllib¹³, BeautifulSoup¹⁴, Sunpy (The SunPy Community et al. 2020), Datetime¹⁵, Scipy (Jones et al. 2001–), Helioviewer (Ireland et al. 2009)

REFERENCES

¹³ <https://docs.python.org/3/library/urllib.html>

¹⁴ <https://www.crummy.com/software/BeautifulSoup/bs4/doc/>

¹⁵ <https://pypi.org/project/DateTime/>

Astropy Collaboration, Robitaille, T. P., Tollerud, E. J., et al. 2013, A&A, 558, A33, doi: 10.1051/0004-6361/201322068

- Boischot, A. 1957, CRAS, 244, 1326
- Boischot, A., & Clavelier, B. 1968, in IAU Symposium, Vol. 35, Structure and Development of Solar Active Regions, ed. K. O. Kiepenheuer, 565
- Bougeret, J. L., Kaiser, M. L., Kellogg, P. J., et al. 1995, SSRv, 71, 231, doi: [10.1007/BF00751331](https://doi.org/10.1007/BF00751331)
- Brueckner, G. E., Howard, R. A., Koomen, M. J., et al. 1995, SoPh, 162, 357, doi: [10.1007/BF00733434](https://doi.org/10.1007/BF00733434)
- Cane, H. V., & Reames, D. V. 1988a, ApJ, 325, 901, doi: [10.1086/166061](https://doi.org/10.1086/166061)
- . 1988b, ApJ, 325, 895, doi: [10.1086/166060](https://doi.org/10.1086/166060)
- D’Huys, E., Seaton, D. B., Poedts, S., & Berghmans, D. 2014, ApJ, 795, 49, doi: [10.1088/0004-637X/795/1/49](https://doi.org/10.1088/0004-637X/795/1/49)
- Dulk, G. A., & Altschuler, M. D. 1971, SoPh, 20, 438, doi: [10.1007/BF00159777](https://doi.org/10.1007/BF00159777)
- Duncan, R. A. 1981, SoPh, 73, 191, doi: [10.1007/BF00153154](https://doi.org/10.1007/BF00153154)
- Gopalswamy, N. 2004, in Astrophysics and Space Science Library, Vol. 314, Astrophysics and Space Science Library, ed. D. E. Gary & C. U. Keller, 305, doi: [10.1007/1-4020-2814-8_15](https://doi.org/10.1007/1-4020-2814-8_15)
- Gopalswamy, N. 2004, A Global Picture of CMEs in the Inner Heliosphere, ed. G. Poletto & S. T. Suess (Dordrecht: Springer Netherlands), 201–251, doi: [10.1007/978-1-4020-2831-1_8](https://doi.org/10.1007/978-1-4020-2831-1_8)
- Gopalswamy, N. 2011, in Planetary, Solar and Heliospheric Radio Emissions (PRE VII), ed. H. O. Rucker, W. S. Kurth, P. Louarn, & G. Fischer, 325–342
- Gopalswamy, N., Aguilar-Rodriguez, E., Yashiro, S., et al. 2005, Journal of Geophysical Research (Space Physics), 110, A12S07, doi: [10.1029/2005JA011158](https://doi.org/10.1029/2005JA011158)
- Gopalswamy, N., Akiyama, S., Mäkelä, P., Yashiro, S., & Cairns, I. H. 2016, arXiv e-prints, arXiv:1605.02223, doi: [10.48550/arXiv.1605.02223](https://doi.org/10.48550/arXiv.1605.02223)
- Gopalswamy, N., & Kundu, M. R. 1989, SoPh, 122, 145, doi: [10.1007/BF00162832](https://doi.org/10.1007/BF00162832)
- Gopalswamy, N., Mäkelä, P., & Yashiro, S. 2019, Sun and Geosphere, 14, 111, doi: [10.31401/SunGeo.2019.02.03](https://doi.org/10.31401/SunGeo.2019.02.03)
- Gopalswamy, N., Yashiro, S., & Akiyama, S. 2007, Journal of Geophysical Research (Space Physics), 112, A06112, doi: [10.1029/2006JA012149](https://doi.org/10.1029/2006JA012149)
- Gopalswamy, N., Yashiro, S., Michalek, G., et al. 2009, Earth Moon and Planets, 104, 295, doi: [10.1007/s11038-008-9282-7](https://doi.org/10.1007/s11038-008-9282-7)
- Hansen, R., Garcia, C., Grogard, R.-M., & Sheridan, K. 1971, PASA, 2, 57
- Harris, C. R., Millman, K. J., van der Walt, S. J., et al. 2020, Nature, 585, 357, doi: [10.1038/s41586-020-2649-2](https://doi.org/10.1038/s41586-020-2649-2)
- Hillarlis, A., Bouratzis, C., & Nindos, A. 2016, SoPh, 291, 2049, doi: [10.1007/s11207-016-0946-6](https://doi.org/10.1007/s11207-016-0946-6)
- Howard, R. A., Michels, D. J., Sheeley, N. R., J., & Koomen, M. J. 1982, ApJL, 263, L101, doi: [10.1086/183932](https://doi.org/10.1086/183932)
- Howard, R. A., Moses, J. D., Vourlidas, A., et al. 2008, SSRv, 136, 67, doi: [10.1007/s11214-008-9341-4](https://doi.org/10.1007/s11214-008-9341-4)
- Hunter, J. D. 2007, Computing in science & engineering, 9, 90
- Ireland, J., Hughitt, K., Müller, D., et al. 2009, in AAS/Solar Physics Division Meeting, Vol. 40, AAS/Solar Physics Division Meeting #40, 15.01
- Jones, E., Oliphant, T., Peterson, P., et al. 2001–, SciPy: Open source scientific tools for Python. <http://www.scipy.org/>
- Kumari, A., Morosan, D. E., & Kilpua, E. K. J. 2021, ApJ, 906, 79, doi: [10.3847/1538-4357/abc878](https://doi.org/10.3847/1538-4357/abc878)
- Kumari, A., Morosan, D. E., Kilpua, E. K. J., & Daei, F. 2023, A&A, 675, A102, doi: [10.1051/0004-6361/202244015](https://doi.org/10.1051/0004-6361/202244015)
- Kundu, M. R., & Spencer, C. L. 1963, ApJ, 137, 572, doi: [10.1086/147530](https://doi.org/10.1086/147530)
- McKerns, M. M., Strand, L., Sullivan, T., Fang, A., & Aivazis, M. A. G. 2012, arXiv e-prints, arXiv:1202.1056, doi: [10.48550/arXiv.1202.1056](https://doi.org/10.48550/arXiv.1202.1056)
- McLean, D., & Labrum, N. 1985, Solar Radio Astrophysics (Cambridge University Press)
- McMullin, J. P., Waters, B., Schiebel, D., Young, W., & Golap, K. 2007, in Astronomical Society of the Pacific Conference Series, Vol. 376, Astronomical Data Analysis Software and Systems XVI, ed. R. A. Shaw, F. Hill, & D. J. Bell, 127
- Melnik, V. N., Brazhenko, A. I., Konovalenko, A. A., et al. 2018, SoPh, 293, 53, doi: [10.1007/s11207-018-1271-z](https://doi.org/10.1007/s11207-018-1271-z)
- Miteva, R., Samwel, S. W., & Krupar, V. 2017, Journal of Space Weather and Space Climate, 7, A37, doi: [10.1051/swsc/2017035](https://doi.org/10.1051/swsc/2017035)
- Mohan, A., Mondal, S., Wedemeyer, S., & Gopalswamy, N. 2024, arXiv e-prints, arXiv:2402.00185, doi: [10.48550/arXiv.2402.00185](https://doi.org/10.48550/arXiv.2402.00185)
- Morosan, D. E., Kumari, A., Kilpua, E. K. J., & Hamini, A. 2021, A&A, 647, L12, doi: [10.1051/0004-6361/202140392](https://doi.org/10.1051/0004-6361/202140392)
- pandas development team, T. 2020, pandas-dev/pandas: Pandas, latest, Zenodo, doi: [10.5281/zenodo.3509134](https://doi.org/10.5281/zenodo.3509134)
- Patel, B. D., Joshi, B., Cho, K.-S., & Kim, R.-S. 2021, SoPh, 296, 142, doi: [10.1007/s11207-021-01890-6](https://doi.org/10.1007/s11207-021-01890-6)
- Pohjolainen, S., & Talebpour Sheshvan, N. 2020, Advances in Space Research, 65, 1663, doi: [10.1016/j.asr.2019.05.034](https://doi.org/10.1016/j.asr.2019.05.034)
- Robbrecht, E., Patsourakos, S., & Vourlidas, A. 2009, ApJ, 701, 283, doi: [10.1088/0004-637X/701/1/283](https://doi.org/10.1088/0004-637X/701/1/283)

- Robinson, R. D. 1978, *SoPh*, 60, 383,
doi: [10.1007/BF00156538](https://doi.org/10.1007/BF00156538)
- Schmahl, E. J. 1972, *PASA*, 2, 95,
doi: [10.1017/S1323358000013035](https://doi.org/10.1017/S1323358000013035)
- Smerd, S. F. 1970, *PASA*, 1, 305,
doi: [10.1017/S1323358000012030](https://doi.org/10.1017/S1323358000012030)
- . 1971, *Australian Journal of Physics*, 24, 229,
doi: [10.1071/PH710229](https://doi.org/10.1071/PH710229)
- Takakura, T. 1961, *PASJ*, 13, 166
- Takakura, T., & Kai, K. 1961, *PASJ*, 13, 94
- Talebpour Sheshvan, N., & Pohjolainen, S. 2018, *SoPh*, 293,
148, doi: [10.1007/s11207-018-1371-9](https://doi.org/10.1007/s11207-018-1371-9)
- The SunPy Community, Barnes, W. T., Bobra, M. G.,
et al. 2020, *The Astrophysical Journal*, 890, 68,
doi: [10.3847/1538-4357/ab4f7a](https://doi.org/10.3847/1538-4357/ab4f7a)
- Weiss, A. A. 1963, *Australian Journal of Physics*, 16, 526,
doi: [10.1071/PH630526](https://doi.org/10.1071/PH630526)
- Wild, J. P. 1970, *Proceedings of the Astronomical Society
of Australia*, 1, 365, doi: [10.1017/S1323358000012364](https://doi.org/10.1017/S1323358000012364)
- Yashiro, S., Gopalswamy, N., Michalek, G., et al. 2004,
J. Geophys. Res., 109,
doi: <https://doi.org/10.1029/2003JA010282>
- Young, C. W., Spencer, C. L., Moreton, G. E., & Roberts,
J. A. 1961, *ApJ*, 133, 243, doi: [10.1086/147019](https://doi.org/10.1086/147019)
- Zhou, G., Wang, J., & Cao, Z. 2003, *A&A*, 397, 1057,
doi: [10.1051/0004-6361:20021463](https://doi.org/10.1051/0004-6361:20021463)
- Zic, A., Murphy, T., Lynch, C., et al. 2020, *ApJ*, 905, 23,
doi: [10.3847/1538-4357/abca90](https://doi.org/10.3847/1538-4357/abca90)